Geophysical Journal International

Geophys. J. Int. (2015) **200,** 106–110
GJI Seismology

doi: 10.1093/gji/ggu382

EXPRESS LETTER

The traveltime holographic principle

Yunsong Huang and Gerard T. Schuster

Earth Science and Engineering, King Abdullah University of Science and Technology, Thuwal 23955-6900, *Saudi Arabia. E-mail: yunsongh@gmail.com*

Accepted 2014 September 30. Received 2014 September 30; in original form 2014 September 5

SUMMARY

Fermat's interferometric principle is used to compute interior transmission traveltimes τ_{pq} from exterior transmission traveltimes τ_{sp} and τ_{sq}. Here, the exterior traveltimes are computed for sources **s** on a boundary B that encloses a volume V of interior points **p** and **q**. Once the exterior traveltimes are computed, no further ray tracing is needed to calculate the interior times τ_{pq}. Therefore this interferometric approach can be more efficient than explicitly computing interior traveltimes τ_{pq} by ray tracing. Moreover, the memory requirement of the traveltimes is reduced by one dimension, because the boundary B is of one fewer dimension than the volume V. An application of this approach is demonstrated with interbed multiple (IM) elimination. Here, the IMs in the observed data are predicted from the migration image and are subsequently removed by adaptive subtraction. This prediction is enabled by the knowledge of interior transmission traveltimes τ_{pq} computed according to Fermat's interferometric principle. We denote this principle as the 'traveltime holographic principle', by analogy with the holographic principle in cosmology where information in a volume is encoded on the region's boundary.

Key words: Tomography; Interferometry; Computational seismology.

1 INTRODUCTION

Kirchhoff migration and migration velocity analysis require the computation of transmission traveltimes τ_{sp} for sources at $\mathbf{s} \in B$ on the exterior boundary B that bounds all interior points $\mathbf{p} \in V$ in the volume V (Yilmaz 2001). These transmission traveltimes are computed by either a ray tracing or eikonal finite-difference method for each source on the exterior surface B. For this reason, the transmission traveltimes τ_{sp} will be referred to as exterior traveltimes.

Some algorithms for ray-based waveform inversion and IM elimination require the computation of 'interior transmission traveltimes' τ_{pq}, where **p** and **q** are both in the interior volume. This can be computationally expensive because, unlike exterior traveltimes τ_{sp} where the source is on a 2-D surface boundary, the interior transmission traveltimes τ_{pq} are computed for every source point **p** and receiver point **q** in the 3-D volume. To mitigate this expense, we propose to compute τ_{pq} by first calculating exterior traveltimes τ_{sp} and then generating the interior traveltimes τ_{pq} by finding the source s^* that gives the stationary residual $\tau_{s^*q} - \tau_{s^*p} \rightarrow \tau_{pq}$. This follows from Fermat's interferometric principle (Schuster 2005a,b).

2 THEORY

Assume that exterior traveltimes τ_{sp} are computed for all sources **s** on the top boundary in Fig. 1 and all receiver points **p**, **q** in the interior. In this case Fermat's principle for a local minimum says that for a specified pair of interior points **p** and **q** we have

$$[\tau_{sp} + \tau_{pq}] \geq \tau_{sq}, \tag{1}$$

for all $\mathbf{s} \in B$ near the stationary source at $\mathbf{s}^*$. The above equation becomes an equality when $\mathbf{s} \rightarrow \mathbf{s}^*$ and $\tau_{sq} \rightarrow \tau_{s^*q}$. Fermat's principle also holds true for a local maximum, so in this case the $\geq$ symbol is replaced by $\leq$. For example, eq. (1) can be rearranged to give $[\tau_{sq} - \tau_{sp}] \leq \tau_{pq}$, or

$$\max_s [\tau_{sq} - \tau_{sp}] = \tau_{pq}. \tag{2}$$

The stationary value of the residual $\tau_{sq} - \tau_{sp}$ is equal to the desired traveltime τ_{pq} for a wave to propagate between the specified interior points **p** and **q**. This is a convenient way for calculating τ_{pq} when **p** and **q** are given and we do not know the stationary source position $\mathbf{s}^*$ associated with the stationary ray that passes through these two interior points.

3 NUMERICAL EXAMPLE

A numerical example is now used to compute the interior traveltimes τ_{pq} from the exterior traveltimes in eq. (2). Fig. 2(a) shows the 2-D velocity model and the acquisition geometry. In this example the exterior boundary B refers to the top boundary, where the sources reside. We call the interior traveltimes τ_{pq} feasible, if they can be found according to the traveltime holographic principle, that is if the stationary source point $\mathbf{s}^*$ associated with **p** and **q** belongs to B. For the given **p** shown in Fig. 2(a), the τ_{pq} is feasible over a domain of **q** that is horizontally delimited by the dashed lines shown in Fig. 2(a). The traveltimes computed according to the holographic principle are in nearly perfect agreement with the exact traveltimes (Fig. 2b), as the discrepancies (Fig. 2c) are minuscule.

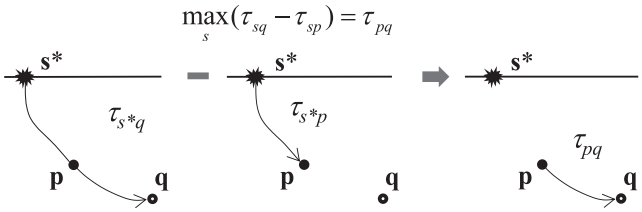

Figure 1. The traveltime τ_{pq} is computed by finding the stationary source position $\mathbf{s}^*$ that gives the stationary residual $\tau_{s*q} - \tau_{s*p}$.

The practical implementation of eq. (2) does not require searching the entire boundary for the stationary source point. The ray between the specified points **p** and **q** can be used to estimate the area on the surface that contains the likely stationary source point. This is the only area that needs to be searched for the stationary point.

4 APPLICATION IN INTERBED MULTIPLE (IM) ELIMINATION

When all interior traveltimes of interest are obtained, an algorithm for IM elimination is made possible. The workflow of this algorithm is as follows.

(1) Migrate the observed data, which contain IMs.
(2) Proceeding from shallow reflectors to deeper ones, delineate pairs of candidate reflectors that may give rise to IMs.
(3) Predict IMs based on such pairs, using the interior traveltimes τ_{pq} computed by invoking the traveltime holographic principle.
(4) Remove the predicted IMs from the observed data by adaptive subtraction.

The prediction in step 3 amounts to finding the traveltime $\tau_{sg}^{\mathfrak{M}}$ of the IM initiating at any source **s** and terminating at any receiver **g**. An example is depicted in Fig. 3, where the task is to find

$$\tau_{sg}^{\mathfrak{M}} = \min_{A,B,C,D,E} \{\tau_{sA} + \tau_{AB} + \tau_{BC} + \tau_{CD} + \tau_{DE} + \tau_{Eg}\}, \qquad (3)$$

for all **s** and **g**. Suppose there are N gridpoints on the top boundary and also on either of the interfaces in Fig. 3. Namely, the numbers of **s**, A, B,... **g** all equal to N, that is $N_s = N_A = N_B = \cdots = N_g = N$. The computational complexity (CC) of eq. (3) is $\mathcal{O}(N_s\, N_A\, N_B\, N_C\, N_D\, N_E\, N_g) = \mathcal{O}(N^7)$. Alternatively, we can build up the desired traveltimes by recursive application of Fermat's principle. This approach, outlined as follows, is analogous to finding the shortest path by dynamic programming (Lew & Mauch 2006).

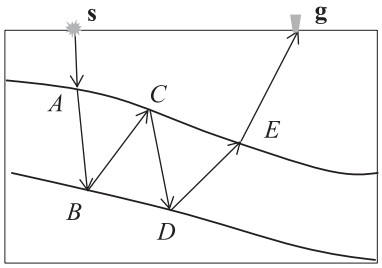

Figure 3. Specular ray path for an interbed multiple (IM) found by recursive application of Fermat's Principle. A–B–C and C–D–E are referred to as V-paths, A–B–C–D–E as the W-path, **s**–A–···–E as the $\mathcal{W}$-path, and **s**–A–···–E–**g** as the $\mathfrak{M}$-path.

(i) For any pair of points A and C on the shallower interface, on the deeper interface find

$$\hat{B} = \arg\min_B \{\tau_{AB} + \tau_{BC}\}, \qquad \tau_{AC}^{\mathrm{V}} = \tau_{A\hat{B}} + \tau_{\hat{B}C}. \qquad (4)$$

This step determines all the V-paths and the associated traveltimes. The specular reflection point $\hat{B}$ tacitly depends on the points A and C. This step involves N^2 invocations of Fermat's principle (for all N^2 pairs of A and C). Each such invocation involves searching over N candidate ray-intersection points (the Bs on the deeper interface in this example) for the minimal traveltime. Taken together, this steps incurs a CC of $\mathcal{O}(N^3)$. The same analysis applies to the remaining steps. In sum, the CC of this 4-step procedure is $\mathcal{O}(N^3)$.

(ii) Determine all the W-paths and the associated traveltimes by minimizing the traveltime of the W-path over C for any given pair of points A and E.

(iii) Determine all the $\mathcal{W}$-paths and the associated traveltimes by by minimizing the traveltime of the $\mathcal{W}$-path over A for any given pair of **s** and E.

(iv) Determine all the $\mathfrak{M}$-paths and the associated traveltimes between **s** and **g** by minimizing the traveltime of the $\mathfrak{M}$-path over E for any given pair of **s** and **g**. This completes both the ray path finding and the traveltime computation by recursive application of Fermat's principle.

We demonstrate IM elimination using the velocity model shown in Fig. 2(a). Step 1 of the workflow produces the migration

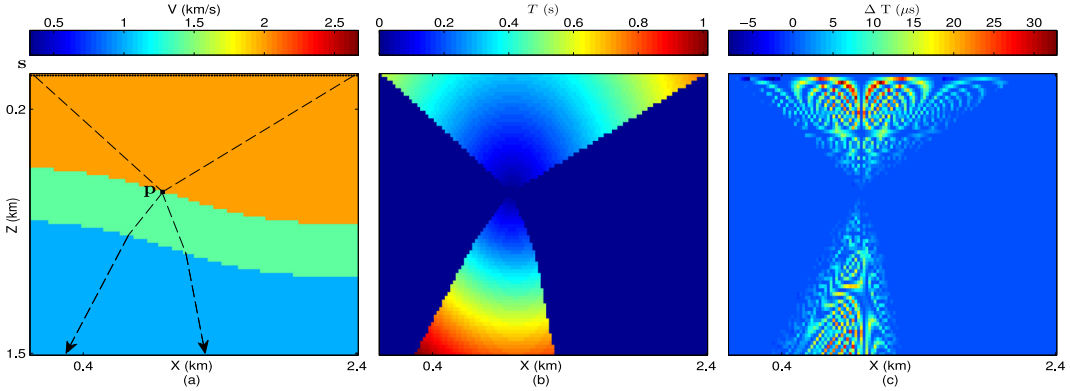

Figure 2. (a) Velocity model, where the 120 sources (dots) evenly distributed on the surface. Dashed lines represent the rays, honouring Snell's law, that connect two of the sources to the internal point **p**. (b) The exact traveltimes τ_{pq} plotted over $\mathbf{q} = (X, Z)$. The dark blue region $\mathcal{I}$ represent infeasible (see text for details) traveltime values. The exact ray-traced traveltimes and the ones obtained according to the holographic principle, as from eq. (2), appear identical, with their negligible difference $\Delta T = T_{\text{holographic}} - T_{\text{exact}}$ plotted in (c).

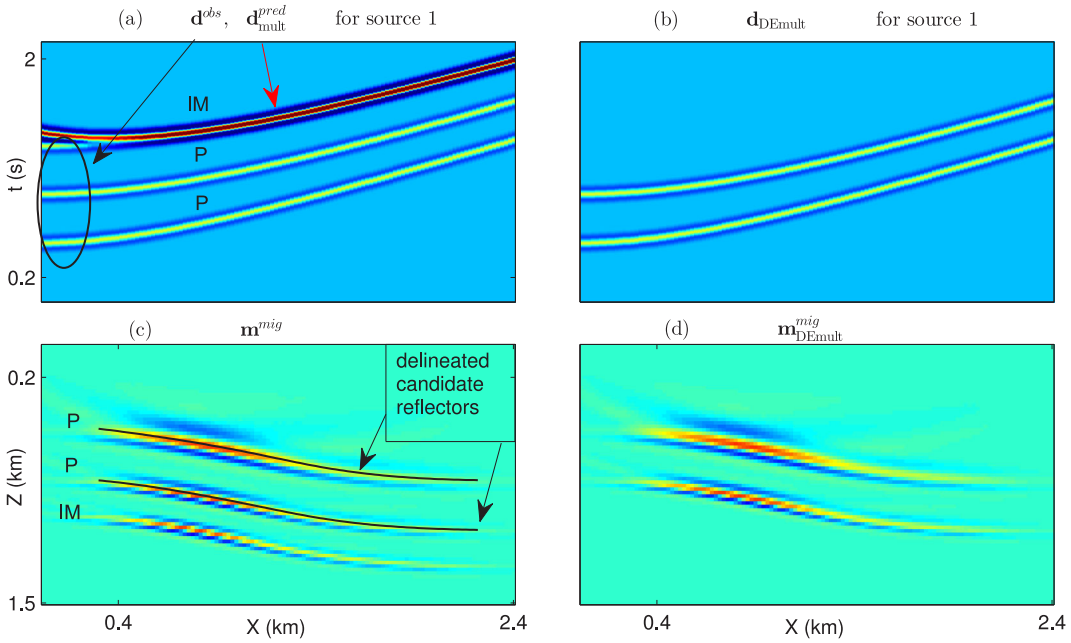

Figure 4. (a) Observed common shot gather (CSG) $\mathbf{d}^{\text{obs}}$, consisting of two primary (P) reflections and an interbed multiple (IM), and $\mathbf{d}^{\text{pred}}_{\text{mult}}$ the predicted IM, of which the amplitude is intentionally exaggerated. (b) After adaptive subtraction, the IM in $\mathbf{d}^{\text{obs}}$ is removed. (c) The migration image computed from all of the observed CSGs. The deepest reflector is an artifact due to the IM in the CSGs. The two shallow reflectors are delineated as candidate generators of interbed multiples. (d) The migration image of the demultipled data, of which one CSG is shown in (b).

image $\mathbf{m}^{\text{mig}}$ (Fig. 4c), from the observed data of which one common shot gather (CSG) is plotted in faint green in Fig. 4(a). Step 2 of the workflow delineates the candidate reflectors in black curves as shown in Fig. 4(c). Note that the left and the right ends of the delineated reflectors are truncated, because the weakly imaged portions of the reflectors are omitted. One example of the IM $\mathbf{d}^{\text{pred}}_{\text{mult}}$ predicted by step 3 of the workflow is plotted in dark red and blue in Fig. 4(a). Observe that at the left end the plotted $\mathbf{d}^{\text{pred}}_{\text{mult}}$ curves upward. This is because of the diffractions, instead of specular reflections, originating at the truncated left ends of the delineated reflectors in Fig. 4(c). The adaptive subtraction in step 4 of the workflow is made easy for this simple example because the source wavelet is assumed to be known and because the primaries and the multiple are well separated. With the proper choice of the allowable time shifts, the observed multiple can be completely removed (Fig. 4b) based on the time-shifted $\mathbf{d}^{\text{pred}}_{\text{mult}}$. If the source wavelet is not known, or if the primaries and multiples overlap, refer to Kaplan & Innanen (2008), Liu *et al.* (2010) and references therein for advanced techniques of adaptive subtraction. Finally, the data devoid of the IM are migrated to produce the image $\mathbf{m}^{\text{mig}}_{\text{DEmult}}$, which contains no artifacts caused by IMs.

5 HOLOGRAPHIC PRINCIPLE

The holographic principle (Bekenstein 2003) is a property of quantum gravity that states that the description of a volume of space can be encoded on the boundary enclosing that region. In other words, a lower-dimensional volume of boundary information can be used to reconstruct a higher-dimensional volume of information, as Bekenstein (2003) writes 'All the information describing the [holographic] 3-D scene is encoded into the pattern of light and dark areas on the two-dimensional piece of film, ready to be regenerated. The holographic principle contends that . . . If a 3-D system can be fully described by a physical theory operating solely on its 2-D boundary, one would expect the information content of the system not to exceed that of the description on the boundary.'

By analogy, Fermat's interferometric principle leads to a 'traveltime holographic principle' in that a 6-D volume of interior traveltimes τ_{pq} can be reconstructed from a 5-D volume of exterior traveltimes τ_{sp}. (Here and hereafter, the position vectors $\mathbf{p}$, $\mathbf{q}$, and $\mathbf{s}$ are of dimensions 3, 3 and 2, respectively.) This is not too surprising since the interior traveltimes are not completely independent of one another, they are connected to their neighbouring times by the eikonal equation to lose a degree of freedom.

Similarly, Green's theorem for acoustic waves can be considered as a waveform holographic principle where 6-D waveform information $\mathcal{G}(\mathbf{p}, t|\mathbf{s})$ on a boundary completely describes the 7-D waveforms $\mathcal{G}(\mathbf{q}, t|\mathbf{p})$ in the interior (van Manen *et al.* 2005, 2006). [Here, $\mathcal{G}(\mathbf{p}, t|\mathbf{s})$ represents the Green's function.] So, the gain of dimensionality is also $7 - 6 = 1$. In fact, the equations for traveltime interferometry (Schuster 2005a,b) are derived by applying stationary phase analysis to the reciprocity equations of correlation type (Snieder 2004).

The computational efficiency of the traveltime holographic principle and the calculation of traveltimes for multipath events are discussed in the appendices.

6 CONCLUSION

Fermat's interferometric principle is used to compute interior transmission traveltimes τ_{pq} from exterior transmission traveltimes τ_{sp}. This is similar to seismic interferometry where interior Green's functions $\mathcal{G}(\mathbf{p}, t|\mathbf{q})$ are computed from exterior Green's functions $\mathcal{G}(\mathbf{p}, t|\mathbf{s})$, except now traveltimes not waveforms are generated. Once the exterior traveltimes are computed, no more ray tracing is needed to compute the interior times so that this interferometric

approach can be more efficient than explicitly computing interior traveltimes τ_{pq} by ray tracing.

For a 3-D model, a 6-D volume of interior traveltimes τ_{pq} can be computed from a 5-D volume of exterior times τ_{sp}, a significant savings in memory requirements. Analogous to the holographic principle in cosmology, Fermat's interferometric principle leads to the traveltime holographic principle.

ACKNOWLEDGEMENTS

This work was supported by King Abdullah University of Science and Technology (KAUST). We thank the sponsors of the CSIM consortium (csim.kaust.edu.sa) for their financial support. We would also like to thank the two reviewers Andrew Curtis and Kees Wapenaar for their insightful comments.

REFERENCES

Bekenstein, J.D., 2003. Information in the holographic universe, *Scient. Am.,* **289**(2), 58–65.

Kaplan, S. & Innanen, K., 2008. Adaptive separation of free-surface multiples through independent component analysis, *Geophysics,* **73**(3), V29–V36.

Lew, A. & Mauch, H., 2006. *Dynamic Programming: A Computational Tool,* Springer.

Liu, Y., Jin, D., Chang, X., Li, P., Sun, H. & Luo, Y., 2010. Multiple subtraction using statistically estimated inverse wavelets, *Geophysics,* **75**(6), WB247–WB254.

Schuster, G., 2005a. Fermat's interferometric principle for multiple reflection tomography, *Geophys. Res. Lett.,* **32**(12), L12303, doi:10.1029/2005GL022351.

Schuster, G.T., 2005b. Fermat's interferometric principle for target-oriented traveltime tomography, *Geophysics,* **70**(4), U47–U50.

Sethian, J.A. & Vladimirsky, A., 2000. Fast methods for the eikonal and related Hamilton–Jacobi equations on unstructured meshes, *Proc. Natl. Acad. Sci.,* **97**(11), 5699–5703.

Snieder, R., 2004. Extracting the Green's function from the correlation of coda waves: a derivation based on stationary phase, *Phys. Rev. E,* **69**(4), 046610.

van Manen, D., Curtis, A. & Robertsson, J., 2006. Interferometric modeling of wave propagation in inhomogeneous elastic media using time reversal and reciprocity, *Geophysics,* **71**(4), SI47–SI60.

van Manen, D.-J., Robertsson, J.O.A. & & Curtis, A., 2005. Modeling of wave propagation in inhomogeneous media, *Phys. Rev. Lett.,* **94,** doi:10.1103/PhysRevLett.94.164301.

Yilmaz, Ö., 2001. *Seismic Data Analysis,* Society of Exploration Geophysicists.

APPENDIX A: COMPUTATIONAL ASPECTS

The CC of traveltime computations by traveltime interferometry are compared to that of a direct method. Let the CC of the former and the latter cases be $C_{\rm HOL}$ and $C_{\rm DIR}$, respectively. Let N_X, N_s and N_M be the numbers of gridpoints along a typical dimension, of sources on the boundary and of points of interest for which all N_M^2 pairs of traveltimes are desired, respectively. Let $C_{\rm EIK}$ be the CC of an eikonal solver for one source. Using the fast marching method (Sethian & Vladimirsky 2000), we have $C_{\rm EIK} = \alpha N_X^2 \log(N_X)$, where α is a proportionality constant. The direct method involves N_M runs of the eikonal solver, suggesting

$$C_{\rm DIR} = N_M\, C_{\rm EIK} = \alpha N_M N_X^2 \log(N_X). \tag{A1}$$

The interferometric approach consists of two steps. First, to prime with N_s runs of the eikonal solver for all the sources on the boundary, and second, to find τ_{pq} according to eq. (2) for all N_M^2 pair of points **p** and **q**. The CC of the first step is $N_s\, C_{\rm EIK} = \alpha N_s N_X^2 \log(N_X)$. In the second step, we find empirically that if point **q** lies close to point **u**, then most probably the stationary point $\mathbf{s}_1^*$ associated with points **p** and **q** lies close to the stationary point $\mathbf{s}_2^*$ associated with points **p** and **u** as well. Namely, having found $\mathbf{s}_1^*$ and starting there, we only need to step over very few sources before finding the stationary source $\mathbf{s}_2^*$ for **q** and **u**. Suppose each such successive search incurs a cost of γ. The CC of the second step can be expressed as $N_s + \gamma(N_M^2 - 1)$, where the first term is for finding the stationary source for the first pair of points, and the second term is for finding the stationary sources for all the remaining pairs. This contrasts with the analysis in Green's function interferometry (van Manen *et al.* 2006), where the cross-correlations of Green's functions have to be summed over the surrounding surface in order to correctly gather all the later arrivals. In traveltime interferometry, however, only the stationary source needs to be identified. This mitigates the CC. Adding the CCs of the two steps of the interferometric approach gives

$$C_{\rm HOL} \approx \alpha N_s N_X^2 \log(N_X) + N_s + \gamma N_M^2. \tag{A2}$$

To find when the interferometric approach is more efficient, namely, $C_{\rm HOL} < C_{\rm DIR}$, inserting $N_M = N_X^\beta$ into eqs (A1) and (A2), and assuming $N_s \propto N_X \gg 1$ leads, after some algebra, to the condition that $1 < \beta \leq 2$. This defines the computational sweet-spot for traveltime interferometry.

APPENDIX B: MULTIPATHING

Traveltime interferometry for a pair of points **p** and **q** assumes that the ray path from the stationary source $\mathbf{s}^*$ to **p** is subsumed in the ray path from $\mathbf{s}^*$ to **q** (or vice versa), as depicted in Fig. 1. This assumption may be violated by multipathing. One such example is shown in Fig. A1(a). Let the first-arrival traveltime between $\mathbf{s}^*$ and **q** be $\tau^{\rm cir}$, that is the τ_{s^*q} along the ray path (green solid curve) that circumvents the low-velocity zone (LVZ), let $\tau^{\rm str}$ be τ_{s^*q} along the straight ray path (green dotted line) that cuts through the LVZ. From the perspective of first-arrival traveltimes, the LVZ is invisible. In this case, traveltime interferometry will underestimate τ_{pq} because in eq. (2) the τ_{sq} takes the value of the first-arrival traveltime $\tau^{\rm cir}$. This is smaller than $\tau^{\rm str}$, which would produce the true value of τ_{pq}. In effect, the inaccuracy of traveltime interferometry stems from omitting the LVZ, that is from increasing the velocity of this anomaly.

Although detailed treatment of multipathing belongs to future work, we outline here the essence of such a treatment.

(1) Detection of multipathing. One can trace the ray between the points of interest, with the initial direction given by the gradient of traveltime (GoT), assuming the traveltime field has been produced by an eikonal solver. This scheme is illustrated in the lower part of Fig. A1(a). If the difference between the ending ray direction (lower red arrow) and the GoT (green arrow) at **q** exceeds a preset threshold, multipathing is detected.

(2) Inclusion of multipathing in traveltime holographic principle. The key is to introduce a boundary B_1, place virtual sources densely on B_1 and calculate the traveltimes from the virtual sources to all model points. This comes at an extra cost for the additional traveltime computation. The traveltime holographic principle can then be applied to the extended boundary set. As an example, consider

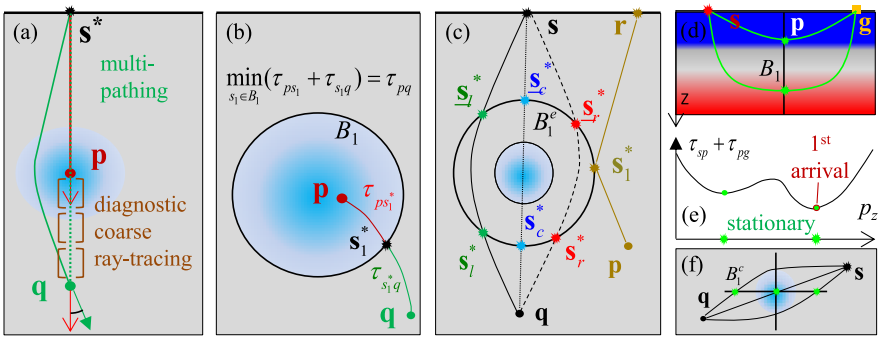

Figure A1. (a) Green solid curve is a shorter traveltime path than green dotted line cutting through the low-velocity zone (LVZ) (cyan disk). Coarse ray tracing (brown brackets denoting the intervals) from **p** to **q**. Upper red arrow and green arrow: the gradients of traveltime. Lower red arrow: ray direction. At **q**, the discrepancy between the red and green arrows suggests multipathing. (b) Computing τ_{pq} by Fermat's principle, if the ray $\overline{\mathbf{pq}}$ intersects boundary B_1. (c) A larger boundary B_1^e encloses the LVZ, such that the multiple paths all intersect B_1^e. The stationary virtual source locations on B_1^e are in pairs (symbols with or without underline). Non-stationary source location (e.g. $\mathbf{s}_1^*$) occurs as a loner. Such non-stationary paths are disregarded in subsequent invocations of traveltime holographic principle. (d) A $v(z)$ velocity model that can give rise to triplication. Given **s** and **g**, there are two stationary ray paths (green curves), but the first-arrival pertains to the deeper curve, overshadowing the shallower one [see the traveltime plot in (e)]. Introducing a vertical boundary B_1 makes both stationary traveltimes explicit. (f) Alternative to B_1^e in (c) is the boundary of a cross B_1^c.

an isolated LVZ. Introduce a boundary B_1 that encloses the LVZ. If both **p** and **q** are enclosed by B_1, τ_{pq} can be found by standard traveltime interferometry. If **p** and **q** are separated by B_1, τ_{pq} can be found by Fermat's principle, as illustrated in Fig. A1(b). If both **p** and **q** reside outside B_1, a method exists to take into account the multitude of traveltimes along every stationary path, due to the LVZ, between **q** and **s**. This method is explained in Fig. A1(c). Similarly, all the stationary traveltimes between **p** and **s** due to the LVZ are also obtained. Then eq. (2) is applied to all pairs of stationary traveltimes τ_{sq}^i and τ_{sp}^j. The maximal $\tau_{pq}^{\hat{i}\hat{j}}$ over all i and j is taken to be the desired τ_{pq}. In this way, multipathing has been correctly taken into account. Another example of multipathing is depicted in Fig. A1(d). The recommendation is to introduce vertical boundaries B_1 at some horizontal spacing. This allows all stationary traveltimes Fig. A1(e) be considered. Fig. A1(f) shows another method of introducing the boundary for the isolated LVZ. How to delineate the extended boundaries robustly in real world examples warrants future research.

One implication of this curative measure on the CC is that, between each of the N_M points and every source on the boundary, a ray tracing exercise required to find whether the ray intersects with the introduced boundary B_1. Suppose the CC for ray tracing is ρN_X, then the total ray tracing cost is $\rho N_M N_s N_X$. The addition of this cost to C_{HOL}, however, does not change the resulting condition following eq. (A2) if $N_s \propto N_X \gg 1$, because this cost $\propto N_M N_X^2$ is smaller than C_{DIR} as given in eq. (A1). Another implication is the cost invoked by 'detection of multipathing'. Since ray tracing between arbitrary pairs of points would defeat the proposal of this letter, we argue that this safeguard measure can still function in checking with much sparser points of interest on a coarser grid, combined with application-dependent rules of thumb.